A Method to Characterize Rat Hindlimb Mechanics Using Dynamic Perturbations

Zhong Wang[1], Sam Tran[1], Gil Serrancolí[2], and Matthew C. Tresch[3,4,5(✉)]

[1] Department of Neuroscience, Northwestern University, Chicago, IL 60611, USA
[2] Department of Mechanical Engineering, Universitat Politècnica de Catalunya, Barcelona, Spain
[3] Department of Biomedical Engineering, Northwestern University, Evanston, IL, USA
m-tresch@northwestern.edu
[4] Department of Physical Medicine and Rehabilitation, Northwestern University, Chicago, IL, USA
[5] Shirley Ryan AbilityLab, Chicago, IL, USA

Abstract. Biomechanical properties, including elasticity, viscosity, and inertia, determine the forces necessary to produce movements. Understanding motor control strategies used by small animals requires knowledge of these properties and their relative importance in motor control. This study established a technique to dynamically perturb the rat hindlimb to determine hindlimb mechanics across a range of configurations. We used a linear motor with high acceleration and precise position servo control to implement fast transient perturbations. A force/torque transducer was mounted on the motor to record force and torque responses from six degrees of freedom during perturbation. A two-camera motion capture system was set up to reconstruct the 3D hindlimb kinematics. A deeply anesthetized animal was placed on a platform, and the hind paw was attached to the transducer. The limb was translated by the motor through a pseudorandom binary sequence of rapid movements with small displacements (2mm). We then fit a second-order linear model to parameterize the elasticity, viscosity, inertia, and background forces of the perturbed system. We obtained mechanical parameters from 197 hindlimb configurations in 3 rats measured across their workspace. The linear model captured $R^2 = 0.93 \pm 0.02$, 0.95 ± 0.01, and 0.93 ± 0.02 of the dynamic responses from three rats. Parameter values were consistent across repeated trials, demonstrating the reliability of the estimation process. Similarly, analysis of joint kinematics also showed minimal kinematic redundancy of limb joint angles across repeated perturbations. These preliminary results show that this dynamic perturbation platform can reliably characterize the mechanical properties of rat hindlimbs. The hindlimb characteristics measured with these procedures will be critical to understanding the control strategies during locomotion and other behaviors.

Keywords: Limb Mechanics · Limb Configuration · Locomotion

N. S. Szczecinski et al. (Eds.): Living Machines 2024, LNAI 14930, pp. 452–459, 2025.
https://doi.org/10.1007/978-3-031-72597-5_31

1 Introduction

Understanding the control strategies responsible for complex behavior is one of the fundamental endeavors of many fields, such as neuroscience, robotics, and artificial intelligence. The control strategies used by organisms are adapted to and constrained by the mechanics of the body [1]. The major mechanical forces dominating movement control include inertial, elastic, and viscous forces [2]. For animals such as rats, all three types of forces might play a significant role during behavior, but their relative importance is unclear, as is how they might vary across the range of limb configurations or in different behavioral conditions.

The passive properties of the limb are important for real-world control. Viscoelastic properties of biological systems can maximize kinetic power and enhance movements over motor-driven systems alone [3]. The passive mechanics of the joints are also critical for resisting hyperextension and maintaining joint stability [4]. However, we lack accurate measurements of those passive components for small animals such as rats.

To estimate these mechanical parameters, we established a perturbation platform to evaluate the dynamic responses of rat hindlimbs. We apply small perturbations with minimal disturbance to the limb configuration to obtain stable estimates of limb parameters. The velocity and the acceleration of the perturbations are high enough to excite high-frequency mechanical components such as viscosity and inertia. A second-order linear model was fit to the measured motion and forces of the perturbation to find mechanical parameters.

2 Methodology

2.1 Instrumentation and Surgical Procedures

Perturbation Motor. This platform consists of a body support platform, a linear motor mounted with a compact force and torque transducer, and a two-camera system for motion capture (Fig. 1). We used a 3-phase synchronous brushless motor stage (MKS Instruments, Inc.) which can perform translations with high acceleration and velocity capacity. The maximum acceleration and velocity can reach 20000 mm/s^2 and 500 mm/s. This motor also had a travel range of 200 mm to accommodate a range of configurations. It was driven by a programmable controller that could perform prescribed perturbation sequences. The motor controller exploited a customizable PIDFF (proportion, integral, derivative and feedforward) controller to minimize the following error between the setpoint and actual position.

Force and Torque Transducer. A compact force transducer (mini40, 20 N and 1 Nm range, ATI Industrial Automation) with six degrees of freedom was mounted on the motor stage to measure the interaction forces and torques of the hindlimb during perturbations. An interface plate was mounted on top of the transducer to attach to the animal foot securely with epoxy.

Motion Capture. Two cameras were positioned to estimate 3D limb configurations. We used monochrome industrial cameras with CMOS image sensors of 1.58M effective pixels and a 5-megapixel lens with a focal length of 6mm (The Imaging Source). We

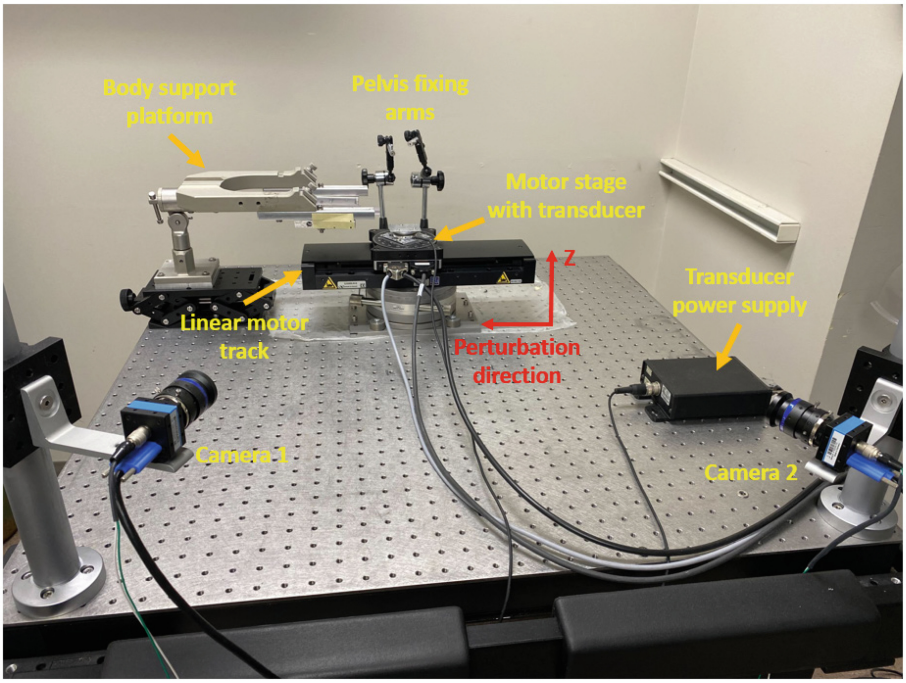

Fig. 1. An overview of the dynamic perturbation platform

captured the hindlimb kinematics with a resolution of 1024 × 768 pixels at 200 frames per second (FPS).

Animal Surgery Procedures. All animal procedures were approved by the Animal Care Committee of Northwestern University. Female Sprague-Dawley rats (250–350 g) were anesthetized with 3% isoflurane with oxygen supply during the surgery and the perturbation experiments. The body temperature was maintained at 36.5 °C using a warming pad and regularly monitored. The depth of the anesthesia was regularly evaluated by pinch reflex. The animal was first implanted with two orthopedic pins into the rostral and caudal ends of the right pelvis. The animal was then transferred to the body support platform, and the two pins were clamped with fixation arms to hold its right pelvis in position while its left limb was perturbed. The left forefoot was attached to the transducer and the motor stage. The following joint landmarks were labeled to be tracked in videos for kinematics and configurations: pelvis top and bottom, hip, knee, ankle, metatarsal, and toe. After the experiments, the animals were euthanized using Euthasol® (Pentobabital Sodium 390 mg/ml & Phenytoin Sodium 50mg/ml).

Perturbation Protocol. In this study, the passive limb mechanics were characterized without reflexive or active control. The left limb was perturbed, while the right limb was immobilized. To minimally perturb the limb, we used a perturbation magnitude of 2 mm (± 1 mm from a neutral position). These fast perturbations are necessary to activate the high-frequency mechanical components such as viscosity and inertia [5].

A pseudorandom binary sequence of forward and backward translations perturbed the hindlimb at one configuration for 40 translations. The limb was then moved by the motor to a new configuration and the sequence repeated. To minimize hysteresis due to stress-relaxation of passive properties, we waited at least 60 s after moving to a new limb position before applying the perturbation sequence.

2.2 Data Acquisition

Data Collection and Synchronization. The kinematics (displacement, velocity, acceleration) of the perturbations were collected from the built-in motor controller interface. The force and torque were transformed from the strain gauge signals and collected using MATLAB. Motion, force, and torque data were synchronized by analog signals and collected at 10000 Hz. Cameras were triggered and synchronized by the analog signals from the motor controller.

Kinematics Analyses. We used the markerless motion capture pipeline DeepLabCut (DLC) to track the body markers on the hindlimb during perturbations [6]. The trained DLC neural network estimated the 2D coordinates for all videos taken by each camera. In addition to the markers on the hindlimb, we also labeled three reference points on the interface plate in order to measure the coordinates of the transducer origin. 2D coordinates from two synchronized cameras were input into the Anipose toolkit to estimate 3D poses [7]. From those triangulated 3D coordinates, we calculated the joint angles of hip, knee and ankle at each time point.

2.3 Model Fitting and Parameter Estimation

We used synchronized displacement and interaction force during pseudorandom binary perturbations to quantify the mechanical parameters. Both signals were fourth-order Butterworth low-pass filtered at 50 Hz.

We fit second-order linear models to parameterize the mechanics. The linear model was as follows:

$$F = m\ddot{x} + c\dot{x} + kx + F_{BG}$$

F stands for force. m, c, k are the identified system inertia, viscosity and elasticity, x is the displacement, and $\dot{x}, \ddot{x}$ are its first and second derivatives velocity and acceleration. F_{BG} is the system background force. We used R^2 to evaluate the quality of model fits.

To evaluate model reliability, we quantified the percent of variation between the parameter estimates from repeated trials.

To estimate the interface mechanical properties, we used the perturbation data without the animal attached to parameterize the interface properties (elasticity, viscosity, and inertia) using the linear model. This model captured the variance of the observed force responses (R^2 of 0.9988 $\pm$ 0.0004) very well and was dominated by inertia, as expected. Using these parameters, we predicted the forces due to the interface during perturbations with the animal attached and subtracted them from all observed forces in order to obtain the forces specifically due to the animal. We then fitted the displacement and animal-specific force (Fig. 2) using the linear model to parameterize rat hindlimb dynamics.

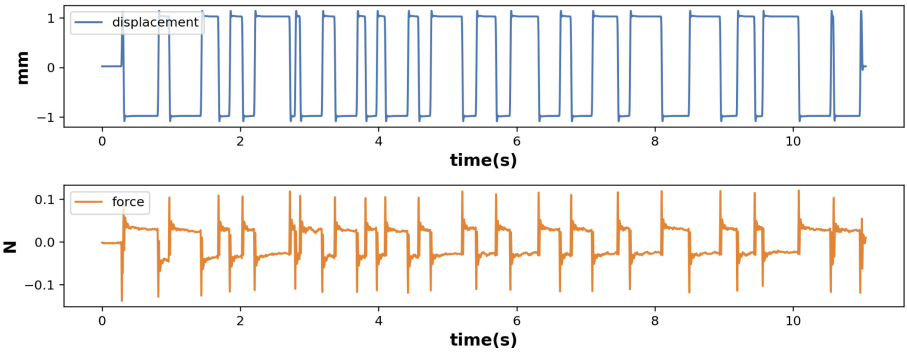

Fig. 2. Displacement and animal-specific force during hindlimb perturbation

3 Results

3.1 Model Fitness and Reliability

To evaluate our experimental setup for estimating rat hindlimb dynamics, we performed perturbations in a total of 197 limb configurations from three rats. A representative trial illustrates that the modeled force captured key features of the measured animal force, especially during the transients (Fig. 3 left). The model score distributions are also shown in Fig. 3. The mean $\pm$ standard deviation of the R^2 scores from all three animals are: Rat1 0.92 $\pm$ 0.02; Rat2 0.95 $\pm$ 0.01; Rat3 0.93 $\pm$ 0.02.

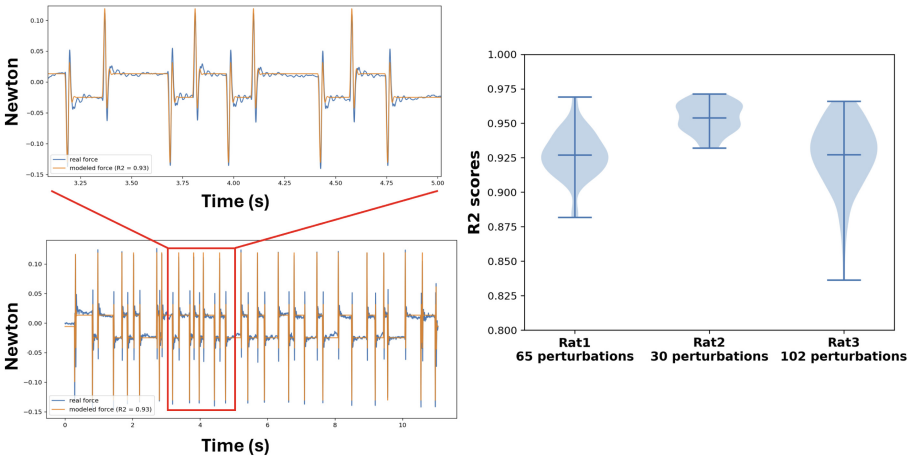

Fig. 3. Comparison between real force and fitted force with one perturbation with $R^2 = 0.93$ (left); Model R^2 scores distributions from three rats (right).

We found that estimates of elasticity, viscosity and inertia were consistent across repeated perturbations. To quantify the differences between repeated measures, we calculated the percentage of variation between the parameters estimated between the two repeated measurements (Fig. 4). Elasticity: $5.4 \pm 3.2\%$; Viscosity: $4.4 \pm 3.4\%$; Inertia: $2.5 \pm 0.8\%$. The variations of each property across repetitions were usually below 10%, indicating the model can generate relatively repeatable system estimates.

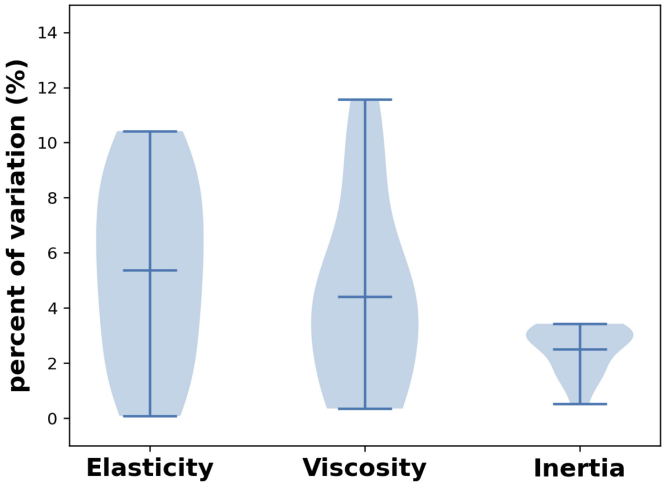

Fig. 4. The percent of variation of all parameters between repeated measures

3.2 Consistency of Limb Configurations Before Perturbations

One issue in these experiments is that, in order to permit free movement of the limb without reaching joint singularities during perturbations, it was necessary to allow internal motion of limb joint angles. As a consequence, there was the potential for variations in limb configuration across perturbation trials, which might lead to poor estimates of limb mechanics. For this purpose, we compared the limb configurations between repeated trials before each perturbation around the same initial configuration (Fig. 5 left), and calculated the joint angle differences between trials across 15 configurations (Fig. 5 right). The between-trial differences in hip angles were $0.46 \pm 0.36°$; knee angles were $0.45 \pm 0.23°$; and ankle angles were $0.32 \pm 0.15°$, suggesting that there were minimal between-trial variations in joint configurations due to kinematic redundancy.

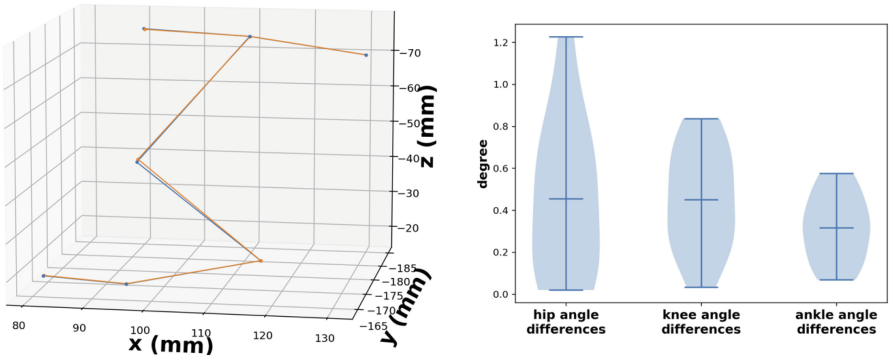

Fig. 5. Configuration comparison between two repeated trials (left). The joint angle differences between repeated trials across configurations.

4 Discussion

In this study, a dynamic perturbation platform was developed to estimate the mechanical properties of rat hindlimbs. The dynamic responses during fast perturbations were used to characterize the elasticity, viscosity and inertia of the system. The model could account for above 90% of the variances in system responses from 197 configurations, and repeated perturbations typically generated similar system parameters with variations of less than 10%. These measures demonstrated the validity and reliability of this technique for measuring the hindlimb mechanics across configurations. In the future, we plan to use this technique to systematically investigate the changes in hindlimb mechanics across the range of configurations used by the animal during different behaviors, such as locomotion. Further, the data obtained from these measurements can be used to evaluate the contribution of passive mechanics to the responses observed during similar perturbations applied to behaving animals. Finally, these parameter estimates and measured data can be used to determine parameters in a detailed musculoskeletal model of the rat hindlimb, choosing muscle model parameters to best match the measured data.

Taken together, these basic measurements of passive rat hindlimb mechanics, along with the platform for performing precise limb perturbations, provide useful information for investigating and interpreting neuromechanical control strategies.

Acknowledgments. We want to acknowledge the generous funding from NSF 2015317 NeuroNex: Communication, Coordination, and Control in Neuromechanical Systems (C3NS) project.

Disclosure of Interests. The authors have no competing interests to declare that are relevant to the content of this article.

References

1. Hogan, N.: Impedance control: an approach to manipulation: part ii—implementation. J Dyn Syst Meas Control. **107**, 8–16 (1985)
2. Sutton, G.P., Szczecinski, N.S., Quinn, R.D., Chiel, H.J.: Phase shift between joint rotation and actuation reflects dominant forces and predicts muscle activation patterns. PNAS Nexus **2** (2023)
3. Ilton, M., et al.: The principles of cascading power limits in small, fast biological and engineered systems. Science **360**, eaao1082 (2018)
4. Villamar, Z., Perreault, E.J., Ludvig, D.: Frontal plane ankle stiffness increases with axial load independent of muscle activity. J. Biomech. **143**, 111282 (2022)
5. Kearney, R.E., Hunter, I.W.: System identification of human joint dynamics. Crit. Rev. Biomed. Eng. **18**, 55–87 (1990)
6. Nath, T., Mathis, A., Chen, A.C., et al.: Using DeepLabCut for 3D markerless pose estimation across species and behaviors. Nat. Protoc. **14**, 2152–2176 (2019)
7. Karashchuk, P., et al.: Anipose: a toolkit for robust markerless 3D pose estimation. Cell Rep. **36**, 109730 (2021)